Korean J. Chem. Eng., **27**(2), 645-650 (2010)
DOI: 10.1007/s11814-010-0057-2

Sintering characteristics of TiO_2 nanoparticles by microwave processing

Sukwon Jung and Jung Hyeun Kim†

Department of Chemical Engineering, University of Seoul, Seoul 130-734, Korea
(*Received 4 March 2009 • accepted 18 June 2009*)

Abstract−In many applications, sintering of particles is required to improve device efficiency. In particular, sintering of TiO_2 nanoparticles attracts great attention because of growing of solar cell applications, and conventional sintering using an electrical furnace has been widely used for sintering of nanoparticles. In this study, conventional and microwave sintering processes were investigated to examine the possibility of application of microwave sintering method to TiO_2 nanoparticles. Microwave sintering of TiO_2 nanoparticles showed promising results compared with the conventional heat treatments in terms of surface area, crystalline phase, optical property and morphology. Considering the short sintering time, the microwave method could be more advantageous than the conventional sintering method in some application areas.

Key words: Microwave Processing, Sintering, TiO_2 Nanoparticle, Anatase, Dye-sensitized Solar Cell

INTRODUCTION

Titania nanoparticles are widely used in various applications such as UV light absorbers in cosmetics [1] and photocatalysts in purifying wastewater [2-8] because of their large surface area characteristics. Recently, many researches on photovoltaic efficiency have been reported after O'Regan and Grätzel [9] found high efficiency dye-sensitized solar cells (DSSCs) by using nanocrystalline TiO_2 particles.

To use TiO_2 nanocrystalline particles for DSSC applications, heat treatment is a necessary step to interconnect the nanoparticles to the electrode. Generally, these particles are conventionally sintered at 450-500 °C for 30-60 min [10-15]. However, if we can reduce the process sintering temperature and time, it would be good for large-scale production in terms of saving energy and time. In addition, since the excessive connection of the particles could be controlled at low temperature and short time sintering, it likely provides a higher film surface area for higher solar cell efficiency.

Microwave sintering is helpful in view of lower process temperature and shorter sintering time than the conventional sintering method [16,17], and much research for microwave sintering has been reported [18-20]. For these reasons, microwave processing was used in this work as a heat treating process, and we examined property changes by both sintering methods (surface area by BET, connection morphology by SEM, crystalline phase content and crystallite size by XRD, optical behaviour by FTIR and UV-Vis spectroscopy) to consider the microwave process as a possible candidate for preparation of DSSCs.

EXPERIMENTAL

1. Preparation of TiO_2 Pellet

Commercially available TiO_2 nanoparticles (P-25, 15-25 nm) were purchased from Degussa, and pellets with 2 cm diameter were manufactured for sintering experiments. For pellet preparation, a plastic molder having 2 cm diameter and 5 cm height was used under approximately 62 kPa for 1 hour without binder material. The pellets were used in both conventional and microwave sintering processes.

2. Sintering

Conventionally, TiO_2 particles were sintered under 450-500 °C for 30-60 min in order not to have phase transformation. In this study, we applied two types of sintering processes: conventional furnace method (450 °C for 30 min) and microwave method (2.45 GHz and 900 W). For furnace sintering, pellets were stored in the furnace for the experimental condition after the furnace temperature stabilized. For microwave sintering, a microwave oven (LBM 1.2A, Cober electronics, Inc.) was used after installing an infrared thermometer for *in-situ* temperature measurements of the pellet samples. The thermometer (MM3MLVF1L, Raytek) is set on the top of the microwave chamber to help monitor the pellet temperature during sintering processes. This thermometer can be generally used from 100 °C to 600 °C with a standard uncertainty of approximately 1.5%. A sample was located at the bottom of the microwave chamber with the infrared of thermometer focusing on the surface of the sample during microwave irradiation. Sintering time was controlled from 10 minutes to 60 minutes.

3. Characterization

Various techniques were used for characterization of the sintered TiO_2 nanoparticles. A BET (Brunauer-Emmett-Teller) analyzer (NovaWin2, Quantachrome Instruments) was used to evaluate the change of specific surface area after the sintering. All samples were first degassed under low pressure condition (77.0 mmHg) at 250 °C for 1 hr prior to measurements to improve the measurement accuracy.

The change of crystalline phase transformation and crystallite size growth by sintering process was estimated with X-ray diffraction (D8 Discover, Buker AXS) patterns. XRD measurements were performed by using Cu Kα radiation at 40 kV and 40 mA, with a step size of 0.02° and 2 s for the time per step. The measured patterns of the samples were compared with the standard anatase and

†To whom correspondence should be addressed.
E-mail: jhkimad@uos.ac.kr

rutile peaks. Crystalline phase transformation after the sintering step can be analyzed by using a simple relationship as shown in Eq. (1) [21].

$$f = \frac{1}{1+1.26\frac{I_R}{I_A}}, \quad (1)$$

where f is the weight fraction of anatase crystal phase, I_A and I_R are XRD peak intensities of the anatase (25.4°) and rutile (27.5°), respectively. In addition, the growth of crystallite size after the sintering can also be evaluated from Scherrer's formula [22]:

$$t = \frac{0.9\lambda}{B\cos\theta_b}, \quad (2)$$

where t is the crystallite size, B is full width at half maximum (FWHM) of the diffraction peak, θ_b is the angle which satisfies Bragg's law, and λ is the x-ray wavelength.

To investigate the change of optical property of sintered TiO_2 nanoparticles, an FTIR spectrometer (RXI, Perkinelmer) and UV-Vis spectrometer (S-4100 PDA, SCINCO) were used. For the FTIR spectra, sample particles were dispersed in a KBr matrix at 10% of weight. A pellet was then formed by compression at the pressure of about 200 MPa. Spectra of the samples were obtained from 16 scans and a resolution of 4 cm^{-1}. During scanning, nitrogen gas was purged for stable operation. In addition, a UV-Vis spectrometer with integration sphere for diffuse reflectance module was used to observe reflectance. A sample with 100% reflectance was used as a reference. The band gaps were estimated with the UV-Vis spectra using the Kubelka-Munk (K-M) theory [23,24]. According to the K-M theory, the total diffuse reflectance from a semi-infinite layer of material R_∞ is related to the α/s as

$$\alpha/s = F(R_\infty) = \frac{(1-R_\infty)^2}{2R_\infty}, \quad (3)$$

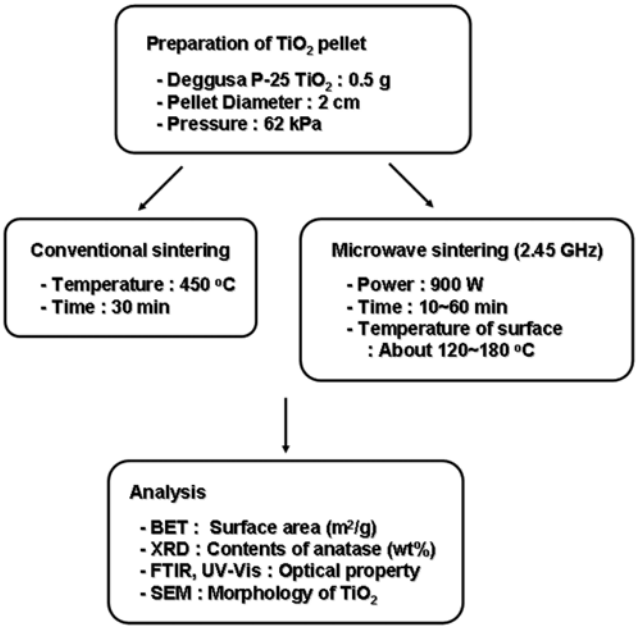

Fig. 1. Flow chart of experimental sequence for TiO_2 nanoparticle sintering.

where α is the absorption coefficient, s is the scattering coefficient, and $R_\infty = R_{sample}/R_{standard}$. $F(R_\infty)$ for any reflectance is called the K-M function.

The morphology of sintered particles was examined with an FE-SEM (S-4100, HITACHI, LTD.). In addition, all photographs were analyzed with the Image-J program [25], which is a public domain Java image processing program from NIH. With this program, we calculated the average area of the sintered particles.

Fig. 1 shows a schematic flow chart of the experimental sequence for conventional and microwave methods. Same analyses were performed for nanoparticles sintered by both methods.

RESULTS AND DISCUSSION

1. Surface Area of Sintered TiO_2 Pellets

Fig. 2 shows the changes of TiO_2 pellet surface temperature and specific surface area with microwave irradiation time. After microwave irradiation, the temperature increased with irradiation time (about 180 °C in 60 minutes). Although the surface temperature of pellets was about 180 °C in 60 minutes, the inside pellet temperature was expected to be higher than the surface because of the thermal gradients the occurred by microwave heating. Fig. 2 also shows the specific surface area of pellets decreased with microwave irradiation time. After 60 minutes, the specific surface area was reduced

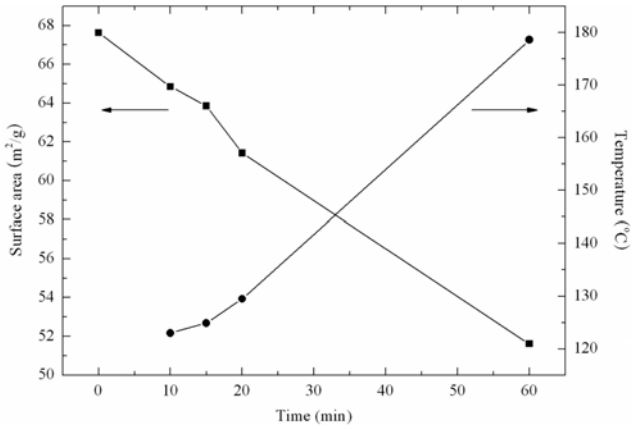

Fig. 2. Influence of microwave sintering time on the surface area and the temperature of TiO_2 pellet.

Table 1. Characteristics of the before- and after-sintered TiO_2 particles

	Before sintering	Conventional sintering	Microwave sintering
Surface area (m^2/g)[a]	67.63	65.74	63.86
Anatase content (wt%)[b]	83.51	82.62	83.43
Crystallite size (nm)[b]	18.09	18.50	19.38
Band gap (eV)[c]	3.243	3.243	3.263
Average area (nm^2)[d]	658	697	717

[a]These values were obtained from BET
[b]These values were calculated from XRD patterns
[c]These values were obtained from UV-Vis spectroscopy
[d]These values were computed from Image-J program

about 24% compared with a before-sintered one. It is considered that even if the surface pellet temperature sintered by microwave was lower than that by conventional way, connections between TiO_2 nanoparticles were well formed due to the generation of heat from the inside of the pellets. Furthermore, when the microwave irradiation time was 15 minutes, the specific surface area was similar to the result of conventional sintering for 30 minutes. The specific surface areas of TiO_2 pellets before-sintered, conventionally sintered, and sintered by microwave are listed in Table 1. From these results, a microwave sintering process would shorten the sintering time and it can be considered as a possible way of manufacturing DSSCs.

2. XRD Analysis

In general, the anatase phase is preferred when TiO_2 particles are utilized as electrode in DSSCs. The anatase phase does not absorb visible light so that all visible light can be used in dye excitation. Consequently, the crystalline phase change has to be confirmed after sintering. In Fig. 3(a), the XRD patterns of the pure anatase (Aldrih, 99.8%) and rutile (Sigma-Aldrich, 99.9%) are shown as well as before-sintered and sintered particles. P-25 (before-sintered) particles mostly consist of anatase phase with a little rutile phase. The weight fraction of anatase in P-25 particles calculated by Eq. (1) was 83.5%. Also, the weight fractions of conventionally sintered and microwave sintered particles were 82.6% and 83.4%, respectively. The results demonstrated that the anatase content was not reduced for both methods, and microwave sintering could be used for nanoparticle sintering process with reduced sintering time.

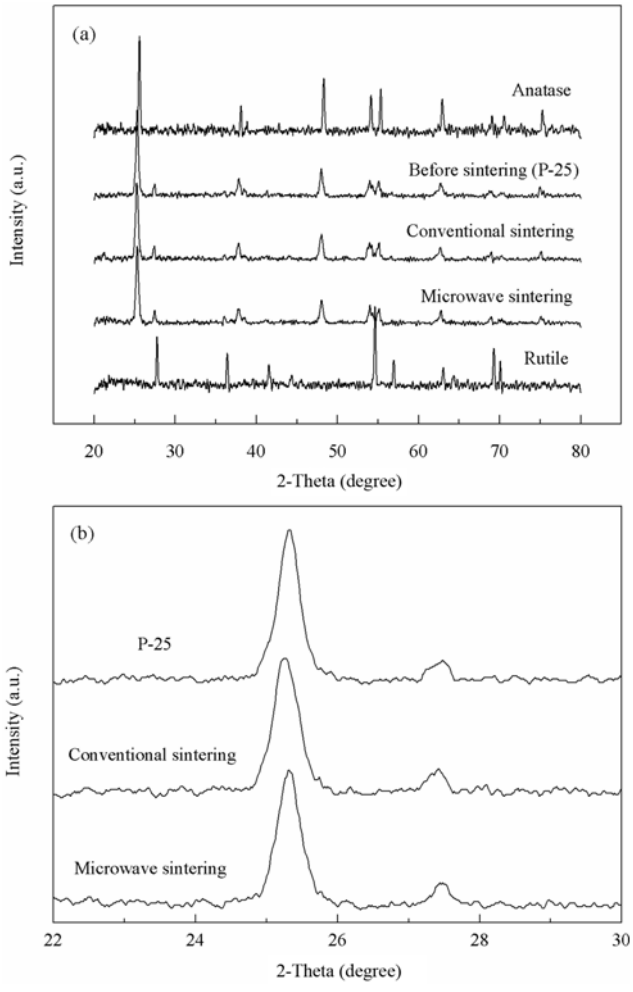

Fig. 3. X-ray diffraction patterns of various TiO_2 particles (a) and enlarged XRD spectra for range from 22° to 30° (b).

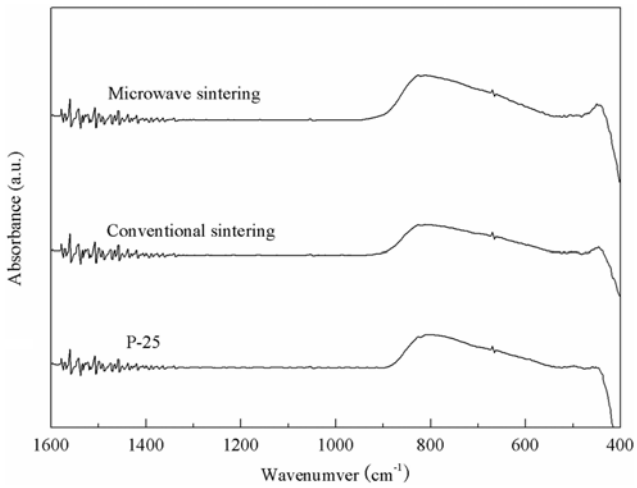

Fig. 4. FTIR spectra of various TiO_2 particles before and after sintering.

To see detailed changes between before-sintered and after-sintered particles, the XRD patterns ranging from 25.4° to 27.5° were enlarged as shown in Fig. 3(b). A peak shift was not observed, but it was able to see that the full width at half maximum (FWHM) at 27.5° was reduced after sintering, which means the crystallite size increased after sintering. So the crystallite sizes of before-sintered and after-sintered particles were calculated for the anatase major peak (25.4°) by Eq. (2), and these results are listed in Table 1. The crystallite size was slightly increased after sintering, and microwave sintering showed more increase of the size than by the conventional method.

3. Optical Properties

The FTIR spectra of TiO_2 samples before-sintering and after-sintering are shown in Fig. 4. Though the changes of FTIR spectra between before- and after-sintering TiO_2 are not shown clearly, the overall peak intensity from 400 to 900 cm^{-1} is slightly increased by both sintering methods. It is possibly attributed to the crystal growth during sintering processes, and it is well matched with the results of crystal sizes after sintering as demonstrated in Table 1.

Kubelka-Munk treated diffuse reflectance spectra for the before- and after-sintering TiO_2 particles are illustrated in Fig. 5, and the band gaps of each TiO_2 samples were calculated by extrapolating a straight line to the x-axis. The band gaps are also summarized in Table 1. The band gap energy of anatase crystalline phase is usually higher than that of rutile phase, and so it is more appropriate for solar cell applications. Our measurements of the band gap energies of anatase and rutile TiO_2 samples were also consistent with the trend. After TiO_2 particles were sintered by both methods, there were no big changes in the band gap energies, because the band gap energy is generally a function of material composition and the crystal size.

4. Morphology of Sintered TiO_2 Particles

Fig. 6 shows SEM Images of TiO_2 nanoparticles before-sintering (a) and after-sintering (b) by microwave and their images processed with the image-J program. The Image-J program accessible

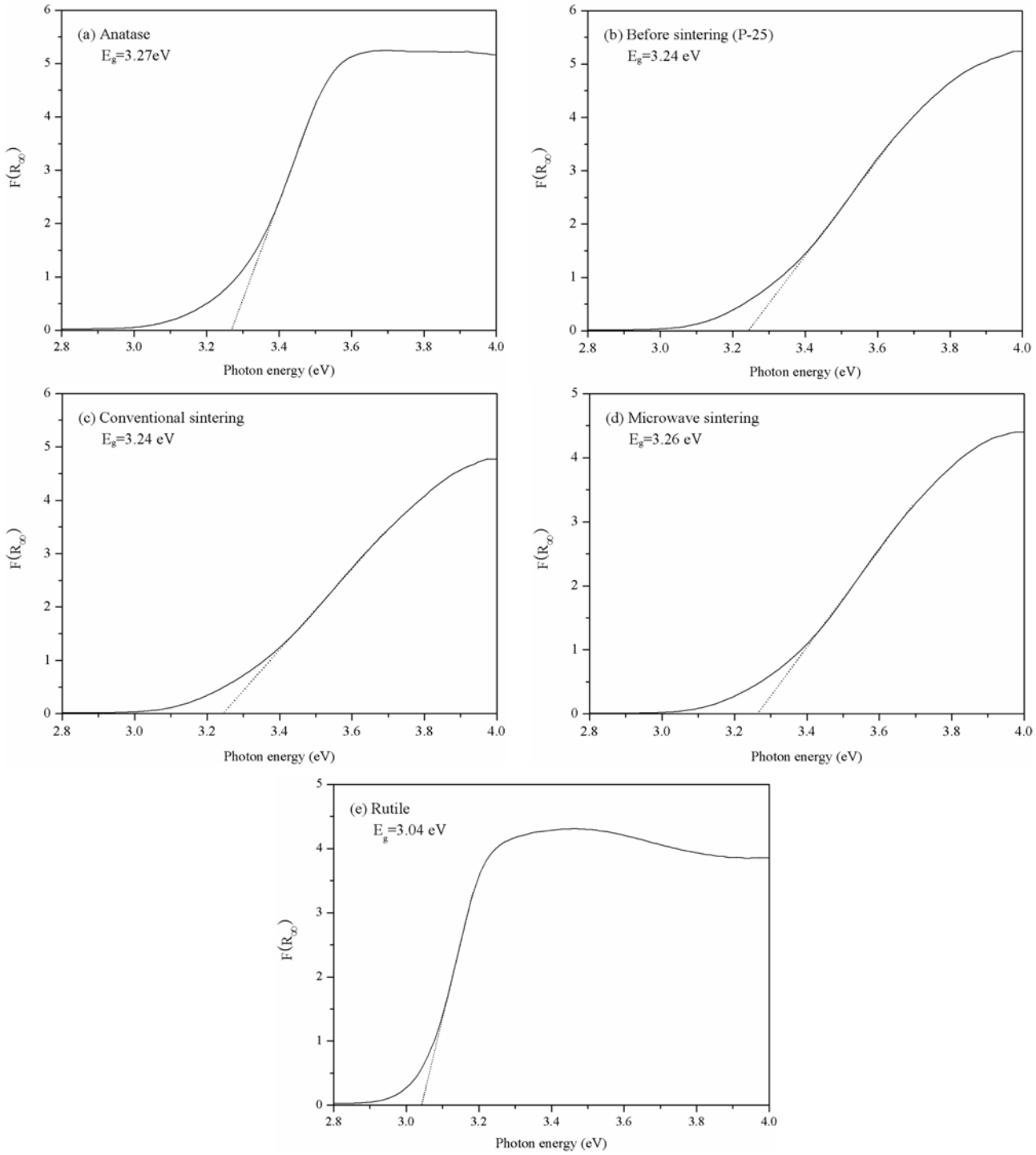

Fig. 5. Kubelka-Munk transformed reflectance spectra of various TiO_2 particles.

at NIH (National Institute of Health, US) was used to see delicate changes of particle connections by the sintering process. The black area in Fig. 6(c) and (d) represents connected particles, and so the extent of sintering can be fairly seen.

The Image-J can help in analyzing an average sintered particle area in the images by selecting boundaries of black areas shown in Fig. 6(c) and (d), and then it counts the number of discrete black parts with calculating total areas of black ones. After this process, with the purpose of obtaining an average connected particle area, the total areas were divided by the number of black parts counted. These values are summarized in Table 1. These numerical values indirectly suggested the extent of particle connections by sintering. If there are no networks between particles after sintering, the average size would be about 490 nm^2 (the area of circle with 25 nm diameter). However, the particles in the pellet cannot exist individually after compression. Therefore, the average size (658 nm^2) of particles

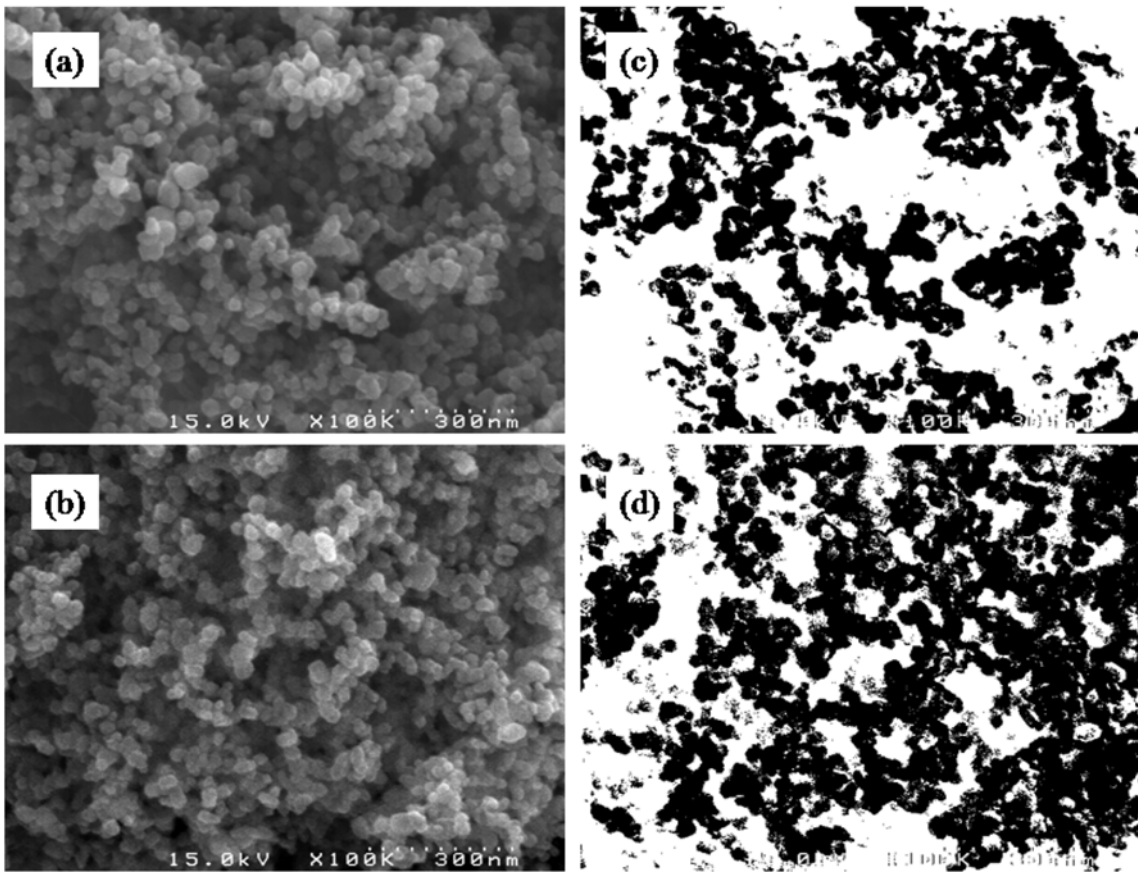

Fig. 6. SEM photographs of TiO_2 particles with (a) before-sintering and (b) after microwave sintering. SEM images processed with Image-J program (c) before-sintering and (d) after microwave sintering.

before sintering was higher than 490 nm^2. Comparing the average size of connected particles before-sintered with conventionally sintered and microwave sintered cases, the average sizes were increased by 5.9% and 8.9% respectively. Therefore, we understood the formation of a network between particles by microwave sintering with the SEM images, and it coincides with the results of BET analysis.

CONCLUSIONS

Conventional and microwave sintering processes were investigated to examine the possibility of using the microwave method for DSSCs applications. Microwave sintering of TiO_2 nanoparticles showed promising results compared with the conventional heat treatments in terms of surface area, crystalline phase, optical property and morphology. Considering the short sintering time, the microwave method could be much more advantageous than the conventional sintering method.

ACKNOWLEDGMENT

This work was supported by the University of Seoul 2008 Research Fund. The authors also would like to thank Dr. Heedong Jang at Korea Institute of Geoscience and Mineral Resources and professor emeritus Dr. DeokChan Kim at the University of Seoul for their helpful discussions for this article.

REFERENCES

1. J. Glówczyk-Zubek, *J. Appl. Cosmetol.*, **22**, 143 (2004).
2. R. Thiruvenkatachari, S. Vigneswaran and I. S. Moon, *Korean J. Chem. Eng.*, **25**, 64 (2008).
3. H. R. Kim, K. Y. Choi and Y.-G. Shul, *Korean J. Chem. Eng.*, **24**, 596 (2007).
4. W. S. Nam and G. Y. Han, *Korean J. Chem. Eng.*, **20**, 180 (2003).
5. Y.-S. Chai, J.-C. Lee and B.-W. Kim, *Korean J. Chem. Eng.*, **17**, 633 (2000).
6. S. Kuwabata, H. Yamauchi and H. Yoneyama, *Langmuir*, **14**, 1899 (1998).
7. J. L. Ferry and W. H. Glaze, *Langmuir*, **14**, 3551 (1998).
8. J. C. Crittenden, J. Liu, D. W. Hand and D. L. Perram, *Water Res.*, **31**, 429 (1997).
9. B. O'Regan and M. Gratzel, *Nature*, **353**, 737 (1991).
10. J.-W. Lee, K.-J. Hwang, W.-G. Shim, K.-H. Park, H.-B. Gu and K.-H. Kwun, *Korean J. Chem. Eng.*, **24**, 847 (2007).
11. S. Ngamsinlapasathian, T. Sreethawong, Y. Suzuki and S. Yoshikawa, *Sol. Energ. Mat. Sol. C.*, **86**, 269 (2005).
12. M. G. Kang, N.-G. Park and S. H. Chang, *Sol. Energy Mater. Sol. C.*, **75**, 475 (2003).
13. N.-G. Park, J. van de Lagemaat and A. J. Frank, *J. Phys. Chem. B*, **104**, 8989 (2000).
14. M. Gratzel, *Prog. Photovolt: Res. Appl.*, **8**, 171 (2000).

15. C. J. Barbe, F. Arendse, P. Comte, M. Jirousek, F. Lenzmann, V. Shklover and M. Gratzel, *J. Am. Ceram. Soc*., **80**, 3157 (1997).
16. W. H. Sutton, *Am. Ceram. Soc. Bull*., **68**, 376 (1989).
17. D. D. Upadhyaya, A. Ghosh, G. K. Dey, R. Prasad and A. K. Suri, *J. Mater. Sci*., **36**, 4707 (2001).
18. S. A. Borkar and S. R. Dharwadkar, *Ceram. Int*., **30**, 509 (2004).
19. K. H. Brosnan, G. L. Messing and D. K. Agrawal, *J. Am. Ceram. Soc*., **86**, 1307 (2003).
20. J. H. Park and Z. S. Ahn, *J. Mater. Sci*., **30**, 3339 (1995).
21. R. A. Spurr and H. Myers, *Anal. Chem*., **29**, 760 (1957).
22. B. D. Cullity and S. R. Stock, *Elements of X-ray diffraction*, Prentice Hall, London (2001).
23. P. Kubelka, *J. Opt. Am*., **38**, 448 (1948).
24. P. Kubelka and F. Munk, *Z. Tech. Phys*., **12**, 593 (1938).
25. http://rsbweb.nih.gov/ij/index.html